

Optical investigation of osteoarthritic human cartilage (ICRS grade) by confocal Raman spectroscopy: a pilot study

Rajesh Kumar¹ · Kirsten M. Grønhaug² · Nils K. Afseth³ · Vidar Isaksen⁴ · Catharina de Lange Davies¹ · Jon O. Drogset⁵ · Magnus B. Lilledahl¹

Received: 24 May 2015 / Revised: 12 August 2015 / Accepted: 13 August 2015
© Springer-Verlag Berlin Heidelberg 2015

Abstract Biomolecular changes in the cartilage matrix during the early stage of osteoarthritis may be detected by Raman spectroscopy. The objective of this investigation was to determine vibrational spectral differences among different grades (grades I, II, and III) of osteoarthritis in human osteoarthritic cartilage, according to the International Cartilage Repair Society (ICRS) grading system. Degenerative articular cartilage samples were collected during total joint replacement surgery and were classified according to the ICRS grading system for osteoarthritis. Twelve cartilage sections (4 sections of each ICRS grades I, II, and III) were selected for Raman spectroscopic analysis. Safranin-O/Fast green was used for histological staining and assignment of the Osteoarthritis Research Society International (OARSI) grade. Multivariate principal component analysis (PCA) was used for data analysis. Spectral analysis indicates that the content of disordered coil collagen increases significantly during the early progression of osteoarthritis. However, the increase was not

statistically significant during later stages of the disease. A decrease in the content of proteoglycan was observed only during advanced stages of osteoarthritis. Our investigation shows that Raman spectroscopy can classify the different stage of osteoarthritic cartilage and can provide details on biochemical changes. This proof-of-concept study encourages further investigation of fresh cartilage on a larger population using fiber-based miniaturized Raman probe for the development of in vivo Raman arthroscopy as a potential diagnostic tool for osteoarthritis.

Keywords Raman spectroscopy · Osteoarthritis · Cartilage · Collagen · Biomedical optical analysis

Introduction

Osteoarthritis is a musculoskeletal disorder whose origin is not exactly clear. It is believed that the disease affects the quality of articular cartilage, both collagen and other extracellular matrix (ECM) components, as well as the associated underlying bone. Imaging and biochemical analysis of musculoskeletal tissues are essential tools for diagnostics and therapeutic assessment in orthopedics. Although the use of the Kellgren-Lawrence (K/L) score is a widely accepted method [1], several studies have demonstrated the complexity involved in early-stage diagnosis of osteoarthritis [2–6].

Currently used clinical imaging modalities (e.g., CT, MRI) provide unique and often complementary information to the rheumatologist. However, these modalities fail to provide crucial information about the biochemical composition of the ECM at the molecular level. Even though biochemical changes can be correlated with macroscopic features in musculoskeletal disorders [7], a technique that can detect changes at

Electronic supplementary material The online version of this article (doi:10.1007/s00216-015-8979-5) contains supplementary material, which is available to authorized users.

✉ Rajesh Kumar
101rajesh@gmail.com

¹ Department of Physics, Norwegian University of Science and Technology (NTNU), 7491 Trondheim, Norway

² Orthopaedic Department, Levanger Hospital, Kirkegata 2, 7600 Levanger, Norway

³ Nofima, Postbox 210, 1431 Ås, Norway

⁴ Department of Medical Biology, The Arctic University of Norway (UiT), 9037 Tromsø, Norway

⁵ Department of Orthopaedic Surgery, Trondheim University Hospital, 7491 Trondheim, Norway

59 the molecular level during the early stages of disease is still
60 awaited.

61 Over the past decade, light-based vibrational spectroscopic
62 techniques such as Fourier transform infrared spectroscopy
63 (FTIR) and Raman spectroscopy have been employed to study
64 several components of the ECM in musculoskeletal tissues
65 [8–11]. These techniques can be used to obtain information
66 about the biochemical composition and the chemical environ-
67 ment of relevant molecules. However, a major limitation of
68 FTIR is extensive tissue preparation (including dehydration).
69 Raman spectroscopy, on the other hand, provides similar
70 chemical information, potentially in vivo, without any exter-
71 nal labeling or preparation of the tissue [12, 13]. In Raman
72 spectra, a series of peaks correspond to different molecular
73 bonds, which may be assigned to specific molecules. The
74 intensity of these peaks is proportional to the content of the
75 corresponding molecular components. Hence, these spectra
76 serve as biochemical fingerprints of the tissue and can be
77 further analyzed to provide physiochemical information.
78 Furthermore, the technique can be used for imaging with sub-
79 micron spatial resolution [14].

80 Most studies of osteoarthritis using Raman spectroscopy
81 are focused on the analysis of bone [11, 15–20]. Compared
82 to cartilage, some tissue constituents of bones are relatively
83 strong Raman scatterers and hence provide a strong Raman
84 signal for biochemical analysis. However, the underlying
85 bone is exposed only at an advanced stage of osteoarthritis
86 (i.e., ICRS grade IV), so to detect early-stage osteoarthritis
87 in vivo, it is necessary to perform Raman analysis on the
88 articular cartilage rather than on the bone.

89 Over the past few years, several groups have used Raman
90 spectroscopy to analyze the properties of articular cartilage
91 and associated disease [21]. However, most studies have fo-
92 cused on the assignment and the structure of the Raman bands
93 [22, 23] in the articular cartilage. By investigating osteoarthri-
94 tic femoral head sections, Kontoyannis et al. assigned a few
95 Raman bands to illustrate the difference between articular car-
96 tilage and subchondral bone [24]. Lim et al. and Pudlas et al.
97 demonstrated the potential of Raman spectroscopy for the
98 detection of proteoglycan changes in cartilage using an animal
99 model [25, 26]. In a view of clinical relevancy, it is necessary
100 to investigate human cartilage, especially primary osteoarthri-
101 tis, the most common variant. An analysis of differences in
102 human articular cartilage by Raman spectroscopy during pro-
103 gression of osteoarthritis (described by ICRS grade,
104 Electronic Supplementary Material Table S2, [27–29]) is still
105 missing. In case of OA, changes at the molecular level in bone
106 and synovial fluid were shown to occur before the appearance
107 of any macroscopic changes in radiography [7, 17, 23, 30, 31].
108 Investigations of articular cartilage at the molecular level
109 could therefore be important in understanding the underlying
110 mechanism of osteoarthritis. Raman spectroscopy for cell and
111 tissue analysis generally uses visible/near-infrared light.

Therefore, the optics involved in Raman spectroscopy are
compatible with modern clinical arthroscopes. Hence, with
the advancement of technology and development of a minia-
turize Raman probe, the technique of Raman spectroscopy can
be applied in a clinical setting. Our proof-of-concept study
demonstrates the capability of Raman spectroscopy as a po-
tential tool for grading the osteoarthritic cartilage from the
formalin-fixed tissue samples. The aim of our pilot study
was to demonstrate the feasibility of Raman spectroscopy
for the classification and a relative biochemical analysis in
different stages of human osteoarthritic cartilage. In this arti-
cle, we report a Raman spectroscopic investigation in human
osteoarthritic cartilage for (i) the classification of different
stages of osteoarthritic cartilage, (ii) a relative assessment of
change in secondary structure of proteins during progression
of osteoarthritis, (iii) a relative assessment of proteoglycan
content, and (iv) a quantitative relationship between two stan-
dard clinical grading systems (ICRS vs. OARSI) of
osteoarthritis.

Materials and methods

Confocal Raman microspectrometer

Raman spectra were acquired using a commercial upright
confocal Raman microscope (LabRam HR800 HORIBA
Jobin Yvon). Briefly, the Raman system was equipped with
a 632.10 nm laser used for excitation and was coupled con-
focally to a spectrograph with a focal length of 800 mm
equipped with a grating of 600 g/mm. The laser light was
tightly focused using an Olympus ×60, 1.2 NA, water-
immersion objective. Scattered Raman photons from the
sample were collected in the backscattered geometry by
the same microscope objective, passed through a slit-width
of 100 μm, and collected by the spectrometer, resulting in a
spectral resolution of ~2 cm⁻¹. The spectrometer was
equipped with an air-cooled deep depletion CCD array de-
tector (1024×256 pixels). The laser power at the tissue sur-
face was 8 mW. The spectra were calibrated to a standard
silicon reference peak at 520.7 cm⁻¹.

Sample preparation and classification

The use of human tissues in this study was approved by the
Regional Committee for Medical Research Ethics (2013/265
REK, Norway), and patient’s informed consent was obtained.
Articular cartilage samples were obtained from osteoarthritic
patients undergoing total knee replacement surgery. It was
confirmed that no patient had suffered any injury and had
undergone other prior surgery. Raman spectra were acquired
from the 12 cartilage sections that were collected from the
knee of 3 patients. Four cartilage sections of International

159 Cartilage Repair Society (ICRS) grade I, four cartilage sections of ICRS grade II, and four cartilage sections of ICRS grade III were obtained. The contribution of each patient in collection of cartilage sections is shown in the Electronic Supplementary Material Table S1. All samples were harvested from the femoral condyle of the knee during total knee replacement surgery (arthroplasty). The spectra of bone can easily be differentiated from those of cartilage; hence, ICRS grade IV (exposed bone) was not included in the study. Additionally, a total of 21 samples (including the tissues used for Raman analysis) were collected for histological evaluation. The grading of osteoarthritis was based on the standard ICRS classification shown in the Electronic Supplementary Material Table S2. The assignment of ICRS grades were performed by two experienced orthopedic surgeons, who were blinded to the classification of each other. Only samples assigned a similar ICRS grade by both orthopedic surgeons were included in this study. A representative image of cartilage of ICRS grades I, II, and III obtained from a patient is shown in the Electronic Supplementary Material Fig. S2.

179 The cartilage samples were dissected with a surgical scalpel, perpendicular to the articular surface (from the superficial layer to the subchondral bone) in a cubical shape whose sides were approximately 3–4 mm, fixed in formalin, and stored at 4 °C. For articular cartilage, formalin fixation is recommended by the Histology Endpoint Committee of the ICRS [32]. Previously, it was found that formalin fixation has little effect on vibrational spectra of matrix proteins [33], and it does not cause significant alterations in the Raman spectra of tissues [34–36, 22]. In general, the major change that was observed due to formalin fixation was overall decrease in intensity of spectral peaks [37]. We performed a relative analysis (based on the ratio of peak intensity) in osteoarthritic samples. Therefore, overall reduction in spectral intensity is not a critical issue in our investigation. Moreover, as recommended by Huang et al. [37], to minimize any fixation artifacts, the cartilage sections were thoroughly washed in phosphate-buffered saline (PBS) before Raman measurements. Samples were placed on a small petri dish in such a way that the subchondral bone was at the bottom of the petri dish and the superficial layer of the cartilage was facing the microscope objective. The petri dish was filled with PBS in order to prevent dehydration of the cartilage during measurement. The sample was stable on the surface of the petri dish throughout the measurement. The uppermost exposed articular surface was kept in focus during data acquisition. The data were collected, at randomly chosen points on the articular surface of the cartilage. During random selection of the points, there was sometimes slight change in focus observed due to inherent curvature of the articular surface. However, the observed change in focus was very little. In order to compensate any change in focus and acquire the high-quality spectra, re-focusing was performed, whenever required. The associated background signal

(from PBS) was collected separately at each different focus for data pre-processing.

Spectral acquisition and data analysis

The pre-processing of spectra and data analysis was performed in Matlab (The MathWorks, 2014). The intensities of vertical pixels of CCD were binned to generate the Raman spectra [38]. Subsequently, the unavoidable spurious spikes in the Raman spectra due to cosmic rays were removed by applying the median filter to the raw data set [39]. Because the raw spectra obtained from each tissue sample were composed of Raman signals, autofluorescence and several noise components, the mean of the corresponding background spectra that was acquired from the surrounding medium (PBS) was subtracted from the raw data to remove the interfering signals. In order to enhance the comparability of spectra [40–44], each spectrum was then smoothed (Savitzky-Golay filter, third order, 9 point), and peak normalization (1004 cm^{-1}) was performed (Electronic Supplementary Material Fig. S3).

Biological tissues are, in general, chemically heterogeneous at the micrometer level, and therefore data acquired from a small focal volume [45, 46] may account for a local variations at the micrometer level. Therefore, a single measurement may not be representative of the chemical composition of the sample as a whole. Therefore, spectra were collected from 27 different locations (as large as practically feasible) (for details please see Electronic Supplementary Material Fig. S1). Furthermore, to find the spectra of each ICRS grade that represent the composition of the bulk sample as a whole, and minimize the biochemical heterogeneity at submicron level [47] including any influence of instrument (and/or ambient) response, 108 spectra were spectrally averaged (see Electronic Supplementary Material Fig. S1) over the number of cartilage sections of same ICRS grade ($n=4$), for every spectral wavelength position. Therefore, finally 27 spectra ($n=27$) of each ICRS grade (I, II, and III) were obtained and subjected to further statistical analysis. Spectral acquisitions were collected over the region $800\text{--}1725\text{ cm}^{-1}$, the fingerprint region of cartilage tissue. The acquisition time for each Raman spectrum was 20 s. To compare the spectra obtained from different ICRS osteoarthritic grades of cartilage, multivariate analysis [48–52] was carried out. Principal component analysis (PCA) was selected to compare data in an unsupervised manner to rule out any subjective bias. For the assessment of diagnostic capability (specificity and sensitivity) and prediction efficiency of Raman spectroscopy for the classification of the tissue, the assignment of ICRS grade was chosen as gold standard. ICRS grading system was chosen as this is commonly used in arthroscopic investigations by orthopedic surgeons.

262 **Histological staining**

263 Aggrecan, the core protein of proteoglycans in cartilage, is
 264 bound to a large number of glucosaminoglycans (GAGs).
 265 Safranin-O is a basic dye that binds to the acidic GAGs and
 266 appears orange in color [53]. Safranin-O/Fast Green staining is
 267 preferred over standard H&E staining because the former pro-
 268 vides qualitative information about the proteoglycan content.

269 After Raman spectroscopy measurement, each tissue was
 270 stored in 10 % neutral-buffered formalin (NBF), dehydrated,
 271 and embedded in paraffin. The tissue was sectioned perpen-
 272 dicular to the articular surface and mounted on glass slides.
 273 The sections were deparaffinized in Tissue-Clear® (Sakura)
 274 and rehydrated using decreasing ratios of ethanol to water.
 275 Slides were stained with Weigert’s iron hematoxylin (Sigma-
 276 Aldrich®) and then rinsed in water before incubation in Fast
 277 Green, differentiated in acetic acid, and stained with Safranin-
 278 O (Sigma-Aldrich®) with a Sakura Tissue-Tek Prisma auto-
 279 matic stainer. Dehydration of the slides was performed using
 280 95 % and absolute ethanol. Tissue-Clear was used, before
 281 mounting the section by Sakura Tissue-Tec Glas automatic
 282 coverslipper. Based on morphological and Safranin-O evalu-
 283 ation, each tissue sample was assigned to a specific
 284 Osteoarthritis Research Society International (OARSI) grade
 285 (Electronic Supplementary Material Table S3) [54].

286 **Statistical analysis**

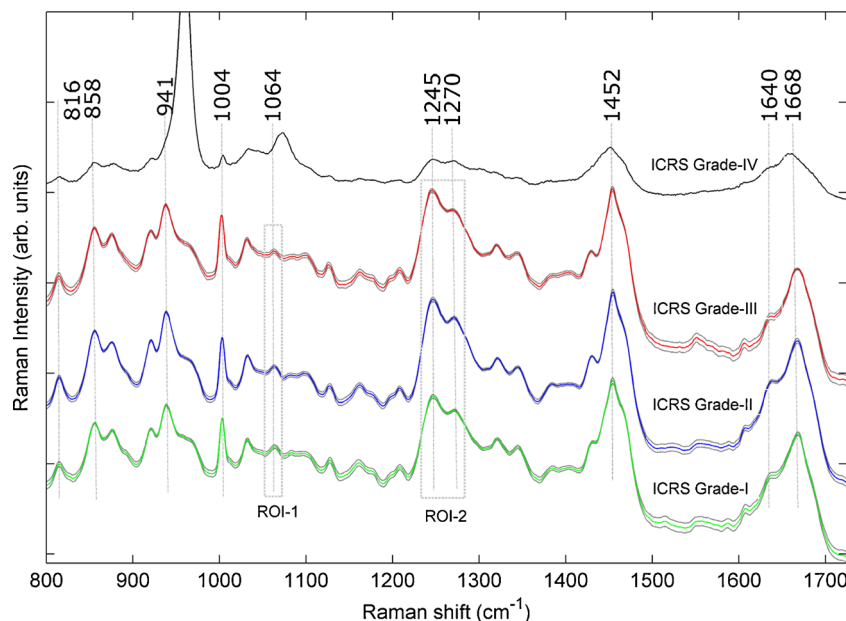
287 The relative change in protein (disordered/ordered) coil con-
 288 tent and proteoglycan content in osteoarthritic articular carti-
 289 lage were investigated by the analysis of region of interest
 290 (ROI)-1 and ROI-2 respectively (Fig. 1). Multiple-group sta-
 291 tistical comparisons among different ICRS osteoarthritic

grades were assessed by nonparametric Kruskal-Wallis 292
 ANOVA test using Matlab (The MathWorks, 2014). In total 293
 108 Raman spectra, 27 representative spectra obtained from 294
 each ICRS grade (i.e., group) of osteoarthritic cartilage were 295
 used for Kruskal-Wallis test. The assumptions (i.e., indepen- 296
 dent measurements, non-normal distribution, and similar vari- 297
 ability) of Kruskal-Wallis test were verified. Box plots dis- 298
 play median values and interquartile ranges. In all multiple- 299
 group pairwise comparisons, a *p* value of less than 0.05 was 300
 considered indicative of statistical significance. The degree of 301
 association between OARSI and ICRS grades was expressed 302
 by the coefficient of determination R^2 , and result was present- 303
 ed as a mean value±standard error using the software IBM 304
 SPSS 21.0 (SPSS Inc., Chicago, Illinois). 305

306 **Results and discussion**

A comparison between the mean (of $n=108$ spectra) Raman 307
 spectra of ICRS grades I, II, and III with standard error is shown 308
 in Fig. 1. Distinguishable Raman bands corresponding to the 309
 different grades of osteoarthritis were observed. These bands 310
 are associated with different vibrational modes of biochemical 311
 components present inside the cartilage matrix [22, 25]. Figure 1 312
 shows the spectra obtained from ICRS grades I, II, III, and IV 313
 tissues. As mentioned in the “Materials and methods” section, 314
 the spectra of bone (grade IV) easily distinguished from the 315
 spectra of cartilage (grades I, II, and III) because of the presence 316
 of minerals (e.g., carbonate peak at 1070 cm^{-1} and phosphate 317
 peak at 960 cm^{-1}) inside bone. Hence, in view of finding spec- 318
 tral differences among degraded cartilage, only cartilage of 319
 grades I, II, and III and without exposed bone (grade IV), which 320
 appears in the advanced stage of osteoarthritis, was analyzed. 321

Fig. 1 Mean ($n=108$ spectra) normalized Raman spectra obtained from ICRS grades I, II, III, and IV tissues. Spectra are offset for clarity. The solid lines indicate the average spectra while the shaded lines represent the standard error. Region of interest (ROI)-1 shows the peak at 1064 cm^{-1} , whereas ROI-2 shows the peaks at 1245 and 1270 cm^{-1} . Separate statistical test was performed for ROIs. The band at 960 cm^{-1} in the spectra from grade IV (black color) is out of scale and hence truncated



322 The loss of proteoglycans in articular cartilage is a hallmark in
 323 the osteoarthritic process. In order to find the changes in content
 324 of proteoglycan in human cartilage, the Raman peak at
 325 1064 cm^{-1} (ROI-1) was chosen because it is the representative
 326 peak of proteoglycan [22, 25, 26]. Change in content of defect-
 327 ive collagen was shown in earlier studies [55, 56]. To find such
 328 changes in ICRS grade of osteoarthritic human cartilage, the
 329 doublet Raman peak at 1245 and 1270 cm^{-1} (ROI-2) were cho-
 330 sen [55–58]. The analyses of two region of interests (ROIs), as
 331 shown in Fig. 1, were performed separately and are described in
 332 the following sections.

333 **Principal component analysis**

334 To determine the classification ability (similarities or differ-
 335 ences among spectra) of Raman spectroscopy, 81 Raman
 336 spectra (27 spectra of each ICRS grades I, II, and III) obtained
 337 from osteoarthritic cartilage were subjected to PCA. PCA was
 338 performed on the raw data matrix by using Matlab (The
 339 MathWorks, 2014). Principal components were obtained by
 340 the eigen-decomposition of covariance matrix which is creat-
 341 ed from the data set [59]. PCA reduces the dimensionality of
 342 the data set by finding an alternative set of co-ordinates [60].
 343 The general form of PCA model is as follows:

$$X = YZ^T + Q \tag{1}$$

346 Where X matrix is decomposed by PCA into two smaller
 347 matrices that are called scores (Y) and loadings (Z). PCA is
 348 performed by the transformation of a large number of corre-
 349 lated variable (i.e., Raman shifts) into smaller number of un-
 350 correlated variables called principal components.
 351 Numerically, it is represented as

$$\sum_{j=1}^J y_{ja} y_{jb} = 0 \tag{2}$$

355 Where y_a and y_b are the a^{th} and b^{th} column of Y matrix,
 356 respectively and

$$\sum_{j=1}^J z_{ja} z_{jb} = 0 \tag{3}$$

360 Where z_a and z_b are the a^{th} and b^{th} rows of Z matrix,
 361 respectively.

362 The first principal components (PC1) account for the max-
 363 imum variability of the dataset. Each succeeding component
 364 (PC2, PC3, etc.) accounts for progressively smaller amounts
 365 of variance. The results of the PCA analysis are shown in
 366 Figs. 2 and 3. Figure 2 shows the data plotted against the three
 367 main PCs. Each Raman spectrum is represented by a single
 368 point in the cluster. The color of the data points represents a
 369 specific ICRS grade. The data were observed to cluster into
 370

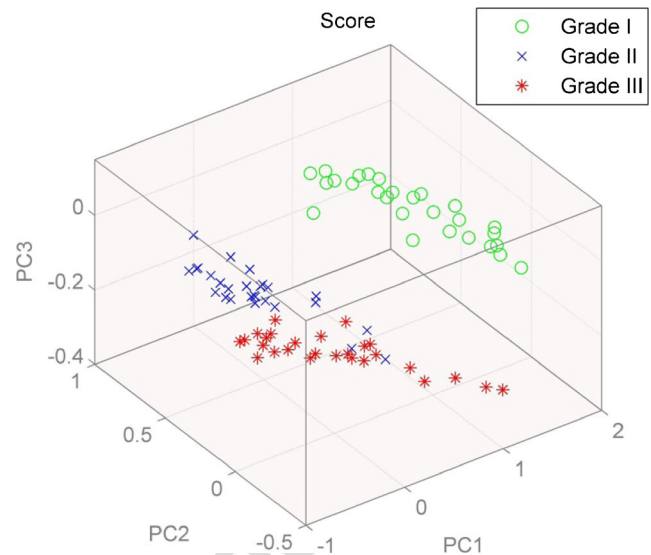


Fig. 2 Multivariate analysis-based PCA algorithm classifies different ICRS grades of osteoarthritis into separate clusters (grade I: green circle, grade II: blue cross, and grade III: red asterisk)

separated groups. Figure 3a–c shows the loading vectors associated with PC-3, PC-2, and PC-1, respectively.

As shown in Fig. 2, the spectra associated with different grades of osteoarthritis appear as distinct clusters when plotted against the three main PCs. In order to discriminate different clusters quantitatively, prediction accuracy was tested by performing leave-one-out cross-validation [60, 61] using Mahalanobis distance as a discriminator. Accordingly, a confusion matrix was constructed which summarizes the correct and incorrect classification of the spectra (Table 1). Each row of the confusion matrix provides the predicted classification for a specific ICRS grade. The diagonal terms of the confusion matrix provide the number of correct predictive classification for the three different ICRS grade. Hence, the average of these diagonal values provides the predictive efficiency of the predictive classification. By the use of confusion matrix, discrimination capability of PCA was calculated in terms of specificity and sensitivity. The specificity for ICRS grades I, II, and III was 87.0, 90.1, and 100 % respectively, while sensitivity was 81.4, 85.1, and 88.8 % respectively. The overall predictive efficiency was approximately 85 %. The high specificity, sensitivity, and efficiency obtained from multivariate analysis on Raman spectra of different ICRS grade demonstrate the potential of Raman spectroscopy as a label free, rapid, and accurate optical tool for classification of the stage of osteoarthritis based on the vibrational spectra of articular cartilage.

To determine the biochemical composition, which is responsible for the separation of the data into three distinct clusters, we plotted the loading spectra (Fig. 3) of the principal components. PC-1, PC-2, and PC-3 explain 84.23, 12.36, and 1.91 % of the total variance in the data set, respectively. Combined, these three PCs explain 98.50 % of the total variation in the data set. Other PCs account for various sources of

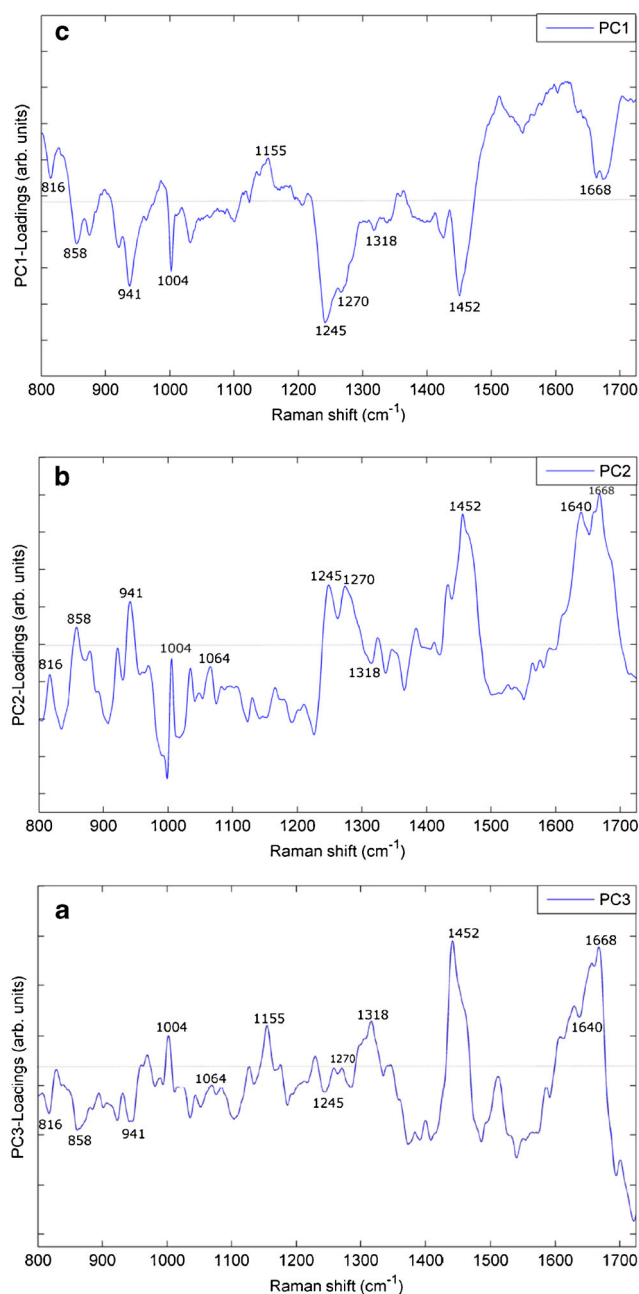


Fig. 3 Loading plot associated with **a** PC 1, **b** PC 2, and **c** PC 3, which are mainly responsible for the discrimination between samples of different grades of osteoarthritis

404 noise in the data set. The loading plots associated with PC-1,
 405 PC-2, and PC-3 shows the spectral features associated with
 406 the cartilage matrix at 1668, 1640, 1452, 1270, 1245, 1064,
 407 1004, 941, 858, and 816 cm^{-1} . Although it is not straightfor-
 408 ward to assign the biochemical Raman peaks associated with
 409 each spectral feature observed in the PC-loading plot, we ten-
 410 tatively assigned the corresponding molecular vibrations
 411 listed in Table 2. Two spectral peaks (1128 and 1321 cm^{-1})
 412 remain unassigned. The origin of these bands is not yet clear
 413 and needs further investigation.

Table 1 Confusion matrix shows the classification for each ICRS grade of osteoarthritic cartilage

Sample	Predicted classification		
	Grade I	Grade II	Grade III
Grade I (27)	22	5	0
Grade II (27)	4	23	0
Grade III (27)	3	0	24

Analysis of relative amide content

Raman spectroscopy is able to provide information about protein structure. Subtle molecular changes often cause detectable vibrational changes that can be detected by Raman analysis [55]. Thus, Raman spectroscopy may be useful in differentiating between normal and pathological cartilage. The doublet Raman peaks at 1245 and 1270 cm^{-1} were shown by ROI-2 in Fig. 1. The intensity ratio of two peaks (I_{1245}/I_{1270}) provides information about the relative content of random vs. ordered coil in the protein structure [55–58].

Figure 4 shows that the median value of the intensity ratio (I_{1245}/I_{1270}) increases with the ICRS grade. To determine whether this ratio varies significantly among different ICRS grades of osteoarthritic cartilage, we performed a nonparametric Kruskal-Wallis ANOVA test; the results are summarized in Fig. 4. Multiple-group pairwise analysis revealed that the median difference was statistically significant ($p < 0.0001$) between grades I and II and between grades I and III but not between grades II and III.

As Fig. 4 indicates that the median value of the intensity ratio (I_{1245}/I_{1270}) increases with the ICRS grade, which means that the ratio of the random to ordered protein coil content changes with the progression of the cartilage disorder. This finding indicates an increase in the content of defective collagen [55] and illustrates the ability of Raman spectroscopy to detect minute modifications in the cartilage structure.

Table 2 Wavenumber (cm^{-1}) and respective vibrational assignment in human articular cartilage [22, 24–26, 57, 58]

Wavenumber (cm^{-1})	Assignment
1668	C-O stretch; amide I- α helix
1640	Amide I- collagen secondary str.
1452	CH_2/CH_3 scissoring; collagen and other protein
1270	(NH_2) bending; amide III-ordered coil
1245	(NH_2) bending; amide III-disordered coil
1064	SO_3^- stretching; glycoaminoglycan
1004	Phenylalanine ring breathing
941	C-C stretching; collagen
858	C-C stretching; proline
816	C-C stretching; protein backbone

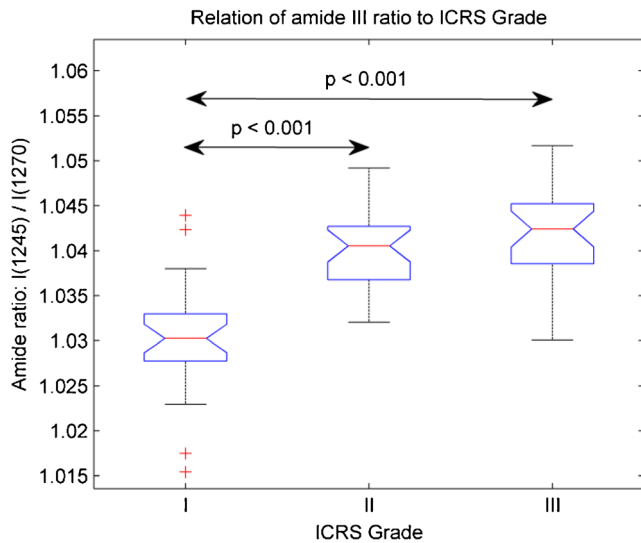


Fig. 4 Comparison ($n=27$ spectra) of relative amide III content in tissues of different grades of osteoarthritis. The dependence of the ratio of random vs. ordered protein coil content is shown as a function of ICRS grade. The symbol “plus sign” represents outliers in the data set

440 However, it should also be noted that although the median
 441 value increases from the grade II group to the grade III group,
 442 the increment is not statistically significant. This result sug-
 443 gests that during the progression of osteoarthritis from grade I
 444 to grade II, the increase in the disordered coil (defective col-
 445 lagen) content is quite high, whereas during the progression of
 446 the disease from grade II to grade III, the increase is not sta-
 447 tistically significant. This trend may arise because during the
 448 early progression of the disease, biochemical changes play a
 449 significant role, whereas later, at more advanced stages of
 450 osteoarthritis, due to the increase in the frictional coefficient
 451 between the contact cartilage surfaces, mechanical effects be-
 452 come more dominant than biochemical effects, and the load-
 453 bearing surfaces start to wear out. Overall, this analysis indi-
 454 cates that the disordered coil content inside the cartilage ma-
 455 trix increases significantly during the early progression of os-
 456 teoarthritis (between grades I and II). However, such incre-
 457 ment was not statistically significant during higher stage pro-
 458 gression of osteoarthritis (between grades I and II). This ob-
 459 servation is in agreement with that made in a previous study
 460 [56]. The relative content of the secondary structure of colla-
 461 gen may play an important role as a biomarker in the early
 462 diagnosis of the disease.

463 **Analysis of proteoglycan content**

464 Proteoglycan is a major component of the ECM in cartilage.
 465 The protein accounts for approximately 40 % of the dry
 466 weight of cartilage and is responsible for providing the osmo-
 467 tic resistance necessary for cartilage to resist compressive loads
 468 [62]. Based on previous reports, we chose the peak at
 469 1064 cm^{-1} as the most representative peak of proteoglycan

[22, 25, 26]. The peak at 1064 cm^{-1} is illustrated by ROI-1
 in Fig. 1. The intensity ratio of the two peaks (I_{1064}/I_{1004})
 provides an indication of proteoglycan content in ECM of
 cartilage because the peak at 1004 cm^{-1} is generally assumed
 to be the most stable Raman peak against any changes in the
 local environment of tissue [63]. To determine the statistical
 significance of the differences in the proteoglycan content
 among the different ICRS grades of osteoarthritic cartilage,
 we performed a nonparametric Kruskal-Wallis ANOVA; the
 results are summarized in the Fig. 5. It shows two results.
 First, there is a decrease in the median value associated with
 proteoglycan content during the progression of osteoarthritis.
 Second, a multiple-group pairwise test reveals that the differ-
 ence between the grades I and II groups is not statistically
 significant, whereas the differences between the grades I and
 III groups and the grades II and III groups are statistically
 significant ($p<0.0001$ and $p<0.001$, respectively).

It has been reported that to compensate for the loss of
 proteoglycan during the progression of joint degenerative dis-
 ease, the synthesis rate of proteoglycan increases during the
 early stages (low grade) of osteoarthritis, whereas it decreases
 in advanced stages (high grade) of disease [64–66]. As indi-
 cated by the results shown in Fig. 5, although there is a de-
 crease in the median value of the proteoglycan content (rep-
 resented by the value of I_{1064}/I_{1004}) during the progression of
 osteoarthritis, the difference between the grades I and II
 groups is not statistically significant, perhaps because the rate
 of proteoglycan synthesis is relatively high during the early
 stages of disease, and hence, the net loss in the proteoglycan
 content may not be sufficiently high to be statistically signif-
 icant between grades I and II.

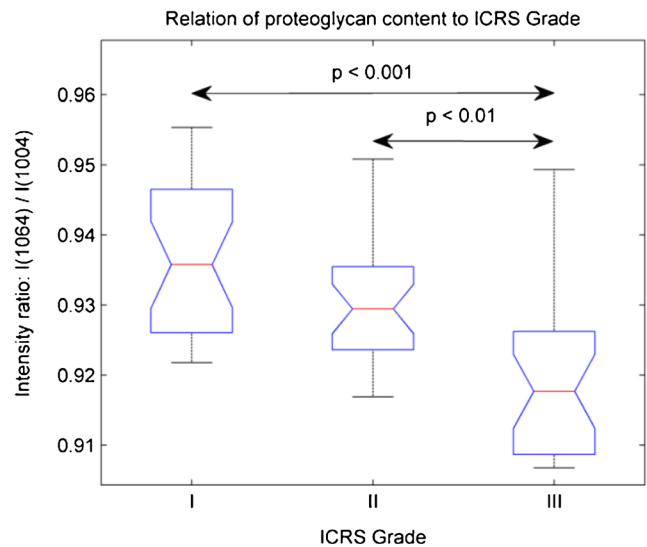


Fig. 5 A relative comparison ($n=27$) of proteoglycan contents in tissues of different grades of osteoarthritis. The dependence of the proteoglycan content inside the cartilage matrix is shown as a function of ICRS grade of osteoarthritis

501 Furthermore, due to the decrease in the synthesis rate of
 502 proteoglycan during the advanced stages of the disease, the
 503 net loss of proteoglycan becomes quite high between grades II
 504 and III and distinctly so between grades I and III. Hence, the
 505 differences between grade II and III and between grades I and
 506 III are statistically significant. In conclusion, by Raman spec-
 507 troscopic analysis, we have shown that the net loss of proteo-
 508 glycan content was only significant at advanced stages of
 509 osteoarthritis. This result is in agreement with previous reports
 510 based on metabolic analysis [64–66].

511 **Histological analysis**

512 A qualitative histological analysis showed higher degradation
 513 of cartilage during progression of osteoarthritis (from ICRS
 514 grade I to grade III). Representative histological images of
 515 ICRS grades I, II, and III are shown in Fig. 6. In sections from
 516 ICRS grade I (Fig. 6a), a thin, pale–green/orange layer shows
 517 the superficial region of the articular cartilage, which appears
 518 smooth with only slight erosions, whereas in sections from
 519 grade II (Fig. 6b), the superficial layer has almost disappeared,
 520 fibers are relatively more fibrillated, and cracks progress down
 521 to the middle zone. Sections from grade III (Fig. 6c) show
 522 significant fragmentation, quite thick fibers in the middle
 523 zone, and cracks propagating down to the deep region.
 524 Sections from grade IV show some remnants of cartilage
 525 and otherwise only exposed bone surface. A clear increase
 526 in morphological disarrangement was indicated by the histo-
 527 logical evaluation with a progressive increase in ICRS grade.

528 To assess the histological images quantitatively, slides were
 529 classified and given a specific grade of osteoarthritis from I to
 530 VI based on the OARSI grading system (Electronic
 531 Supplementary Material Table S3) [54]. Higher OARSI
 532 grades were observed with increasing values of ICRS grade.
 533 The mean OARSI grades for ICRS grades I, II, III, and IV
 534 were 0.92 ± 0.2 , 2.12 ± 0.65 , 3.57 ± 0.25 , and 5.37 ± 0.62 , re-
 535 spectively (Fig. 7). A significant correlation was observed
 536 between the OARSI and ICRS grades ($R^2=0.789$, $p<0.01$).

537 Based on the histological analysis of ICRS grades I, II, and
 538 III, we can conclude that in addition to the progressive thin-
 539 ning of the cartilage (consistent with previous reports
 540 [67–69]), the morphological disorder of collagen fibers in-
 541 creases with ICRS grade, and hence, the results of qualitative
 542 histological evaluation are observed to be in agreement with
 543 the ICRS classification (Electronic Supplementary Material
 544 Table S2) [27–29] of the specimens. Moreover, quantitatively,
 545 a high positive correlation was observed between the results of
 546 ICRS assessment (Electronic Supplementary Material
 547 Table S2) by orthopedic surgeons and those obtained by
 548 OARSI-template-based (Electronic Supplementary Material
 549 Table S3) histological evaluation. This high positive correla-
 550 tion indicates that macroscopic evaluation (e.g., during

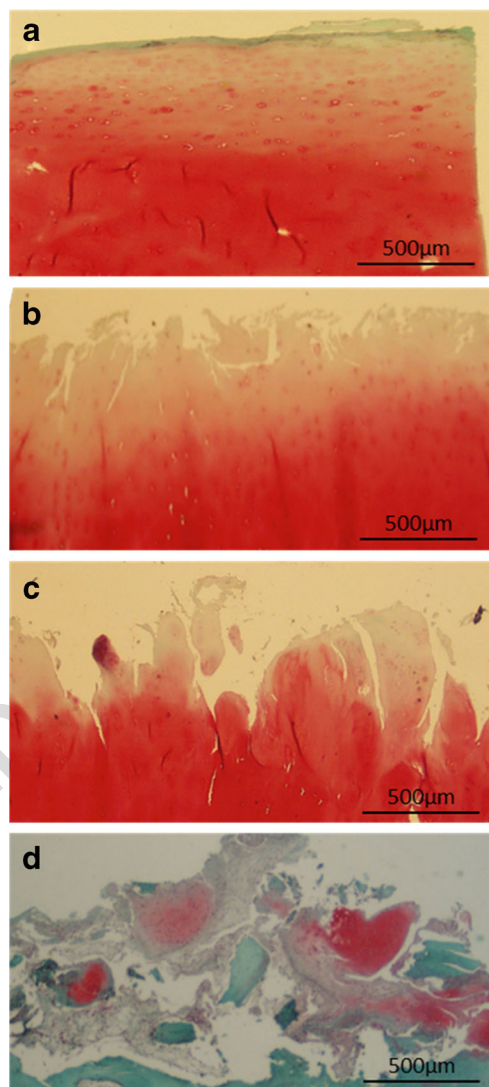


Fig. 6 Histological image of osteoarthritic cartilage stained by Safranin-O/Fast Green. **a** ICRS grade I, **b** ICRS grade II, **c** ICRS grade III, and **d** ICRS grade IV. Distribution of proteoglycan is illustrated in orange/red

surgery or arthroscopy) may be a suitable method for classi- 551
 552 fying degraded cartilage.

Conclusion 553

In conclusion, our study show that Raman spectroscopy 554
 555 could be a potential label-free optical tool which, with high
 556 specificity and sensitivity, can detect the biomolecular
 557 change in human articular cartilage and can classify different
 558 stages (i.e., ICRS grades) of osteoarthritis based on spectral
 559 properties. We were also able to provide information about
 560 the biochemical modification of the cartilage matrix during
 561 the progression of osteoarthritis in terms of the relative con-
 562 tents of ordered and disordered protein coils, which may
 563 potentially serve as biomarker in the early diagnosis of

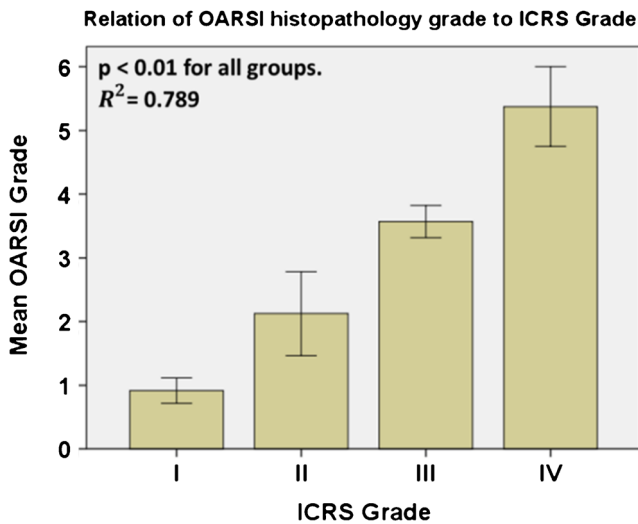


Fig. 7 Mean OARSI grade as a function of ICRS grade of osteoarthritis ($n=21$ cartilage sections). A high correlation exists between the OARSI histological evaluation and macroscopic ICRS assessment

564 osteoarthritis. Moreover, by Raman spectroscopic investigation,
 565 in human model, we have shown that the decrease in
 566 proteoglycan content was clearly observed only in advanced
 567 stage of osteoarthritis. Both of the results, change in protein
 568 content and proteoglycan content, are found to be consistent
 569 with progression of osteoarthritis [56, 64–66].

570 Due to practical reasons, this investigation was performed
 571 in formalin-fixed osteoarthritic cartilage sections and therefore
 572 caution is needed in extrapolation of conclusion to, e.g., fresh
 573 cartilage. Although, the optimum protocol [22, 34–37] developed
 574 to handle the formalin-fixed tissue for Raman spectroscopy
 575 was followed, additional studies are essential to allow
 576 the accurate comparison with fresh cartilage. Further investigations
 577 to determine the effects of various fixatives (e.g., alcohol,
 578 formalin, paraformaldehyde) specifically on vibrational
 579 spectra of cartilage and a comparison with fresh as well as
 580 healthy cartilage are currently under way.

581 The optics involved in Raman spectroscopy are compatible
 582 with modern clinical arthroscopy. Therefore, even though
 583 confocal Raman spectroscopy is still limited to a laboratory
 584 environment, the applied technique can be extended to in vivo
 585 diagnosis with the help of a miniaturized Raman fiber probe
 586 integrated within a clinical arthroscope, which is currently
 587 under development [70]. This pilot study presents a proof-of-concept
 588 investigation in human cartilage; however, to validate the assessment
 589 ability of the proposed spectroscopic method, further analysis on
 590 large number of patients with controls is necessary. Nevertheless,
 591 these results encourage further investigations (e.g., quantitative
 592 determination of biochemical compositions) on human osteoarthritic
 593 cartilage, which may reveal hidden features associated with
 594 progression of the disease. Our ongoing research will focus on
 595 revealing other biochemical information present in Raman spectra,
 596

which may enhance the proposed method’s ability to discern 597
 degraded cartilage even at early stage of manifestation. 598

Acknowledgment We are pleased to acknowledge Kristin G. Sæterbø, 599
 Astrid Bjørkøy, and Ulrike Böcker (Nofima) for their assistance in the 600
 laboratory. The histological analysis was performed at the Cellular and 601
 Molecular Imaging Core Facility (CMIC), Norwegian University of Science 602
 and Technology (NTNU). The partial funding to carry out this study 603
 was received from the joint committee of Helse Midt-Norge (HMN)- 604
 NTNU, Norway. 605

Conflict of interest The authors declare that they have no conflict of 606
 interest. 607
 608

References

609

1. Kellgren JH, Lawrence JS (1957) Radiological assessment of 611
 osteo-arthrosis. *Ann Rheum Dis* 16:494–502 612
2. Kooma PR, Bloem JL, Ceulemans RY, Riyazi N, Rosendaal FR, 613
 Nelissen RG, Carter WO, Hellio Le Graverand MP, Kloppenburg 614
 M (2006) Osteoarthritis of the knee: association between clinical 615
 features and MR imaging findings. *Radiology* 239:811–817 616
3. Li X, Benjamin Ma C, Link TM, Castillo DD, Blumenkrantz G, 617
 Lozano J, Carballido-Gamio J, Ries M, Majumdar S (2007) In vivo 618
 T(1rho) and T(2) mapping of articular cartilage in osteoarthritis of 619
 the knee using 3 T MRI. *Osteoarthritis Cartil / OARS, Osteoarthr* 620
Res Soc 15:789–797 621
4. Raynauld JP, Martel-Pelletier J, Berthiaume MJ, Labonte F, 622
 Beaudoin G, de Guise JA, Bloch DA, Choquette D, Haraoui B, 623
 Altman RD, Hochberg MC, Meyer JM, Cline GA, Pelletier JP 624
 (2004) Quantitative magnetic resonance imaging evaluation of 625
 knee osteoarthritis progression over two years and correlation with 626
 clinical symptoms and radiologic changes. *Arthritis Rheum* 50: 627
 476–487 628
5. Bruyere O, Genant H, Kothari M, Zaim S, White D, Peterfy C, 629
 Burtel N, Richy F, Ethgen D, Montague T, Dabrowski C, 630
 Reginster JY (2007) Longitudinal study of magnetic resonance im- 631
 aging and standard X-rays to assess disease progression in osteoar- 632
 thritis. *Osteoarthritis Cartil / OARS, Osteoarthr Res Soc* 15:98–103 633
6. Cicuttini F, Hankin J, Jones G, Wluka A (2005) Comparison of 634
 conventional standing knee radiographs and magnetic resonance 635
 imaging in assessing progression of tibiofemoral joint osteoarthritis. 636
Osteoarthritis Cartil / OARS, Osteoarthr Res Soc 13:722–727 637
7. Morris MD, Roessler BJ (2006) Future spectroscopic diagnostics in 638
 osteoarthritis. *Fut Rheumatol* 1:383–386 639
8. Bi X, Yang X, Bostrom MP, Camacho NP (2006) Fourier transform 640
 infrared imaging spectroscopy investigations in the pathogenesis 641
 and repair of cartilage. *Biochim Biophys Acta* 1758(7):934–941 642
9. Boskey A, Pleshko Camacho N (2007) FT-IR imaging of native and 643
 tissue-engineered bone and cartilage. *Biomaterials* 28:2465–2478 644
10. West PA, Bostrom MP, Torzilli PA, Camacho NP (2004) Fourier 645
 transform infrared spectral analysis of degenerative cartilage: an 646
 infrared fiber optic probe and imaging study. *Appl Spectrosc* 58: 647
 376–381 648
11. Dehring KA, Crane NJ, Smukler AR, McHugh JB, Roessler BJ, 649
 Morris MD (2006) Identifying chemical changes in subchondral 650
 bone taken from murine knee joints using Raman spectroscopy. 651
Appl Spectrosc 60:1134–1141 652
12. Argyri AA, Jarvis RM, Wedge D, Xu Y, Panagou EZ, Goodacre R, 653
 Nychas G-JE (2013) A comparison of Raman and FT-IR spectroscopy 654
 for the prediction of meat spoilage. *Food Control* 29:461–470 655

656 13. Kumar R, Singh G, Grønhaug K, Afseth N, de Lange DC, Drogset
657 J, Lilledahl M (2015) single cell confocal Raman spectroscopy of
658 human osteoarthritic chondrocytes: a preliminary study. *Int J Mol*
659 *Sci* 16:9341–9353

660 14. Nyman JS, Makowski AJ, Patil CA, Masui TP, O'Quinn EC, Bi X,
661 Guelcher SA, Nicollela DP, Mahadevan-Jansen A (2011)
662 Measuring differences in compositional properties of bone tissue
663 by confocal Raman spectroscopy. *Calcif Tissue Int* 89:111–122

664 15. Kerns JG, Gikas PD, Buckley K, Birch HL, McCarthy ID, Miles J,
665 Briggs TWR, Parker AW, Matousek P, Goodship AE (2013) Raman
666 spectroscopy reveals evidence for early bone changes in
667 osteoarthritis. *Bone Joint J Orthop Proc Suppl* 95-B:45

668 16. Khan AF, Awais M, Khan AS, Tabassum S, Chaudhry AA,
669 Rehman IU (2013) Raman spectroscopy of natural bone and syn-
670 thetic apatites. *Appl Spectrosc Rev* 48:329–355

671 17. Carden A, Morris MD (2000) Application of vibrational spectro-
672 scopy to the study of mineralized tissues (review). *J Biomed Opt* 5:
673 259–268

674 18. Buchwald T, Niciejewski K, Kozielski M, Szybowicz M,
675 Siatkowski M, Krauss H (2012) Identifying compositional and
676 structural changes in spongy and subchondral bone from the hip
677 joints of patients with osteoarthritis using Raman spectroscopy. *J*
678 *Biomed Opt* 17:017007

679 19. Bohic S, Rey C, Legrand A, Sfihi H, Rohanizadeh R, Martel C,
680 Barbier A, Daculsi G (2000) Characterization of the trabecular rat
681 bone mineral: effect of ovariectomy and bisphosphonate treatment.
682 *Bone* 26:341–348

683 20. Notingher I, Jell G, Notingher P, Bisson I, Polak J, Hench L (2005)
684 Raman spectroscopy: potential tool for in situ characterization of
685 bone cell differentiation. *Bioceramics* 17:545–548

Q3 686 21. Boskey AL, Garip S (2012) Diagnosis of Bone and Cartilage
687 Diseases. In *Vibrational Spectroscopy in Diagnosis and*
688 *Screening*, Severcan F, Haris PI (eds). IOS Press: 272–303

689 22. Bonifacio A, Beleites C, Vittur F, Marsich E, Semeraro S, Paoletti
690 S, Sergio V (2010) Chemical imaging of articular cartilage sections
691 with Raman mapping, employing uni- and multi-variate methods
692 for data analysis. *Analyst* 135:3193–3204

693 23. Karen AE (2009) Raman spectroscopy detection of molecular
694 changes associated with osteoarthritis. PhD Thesis, University of
695 Michigan

696 24. Kontoyannis C, Vardaki M, Megas P, Panteliou S, Orkoula M,
697 Papachristou D (2011) Raman spectroscopy of articular cartilage
698 and subchondral bone on osteoarthritic human femoral heads.
699 School of Pharmacy (Publ IP Conference), University of Patras

700 25. Lim NS, Hamed Z, Yeow CH, Chan C, Huang Z (2011) Early
701 detection of biomolecular changes in disrupted porcine cartilage
702 using polarized Raman spectroscopy. *J Biomed Opt* 16(1):017003

703 26. Pudlas M, Brauchle E, Klein TJ, Hutmacher DW, Schenke-Layland
704 K (2013) Non-invasive identification of proteoglycans and chon-
705 drocyte differentiation state by Raman microspectroscopy. *J*
706 *Biophotonics* 6:205–211

707 27. Outerbridge RE (1961) The etiology of chondromalacia patellae. *J*
708 *Bone Joint Surg Br Vol* 43-b:752–757

709 28. Kleemann RU, Krockner D, Cedraro A, Tuischer J, Duda GN (2005)
710 Altered cartilage mechanics and histology in knee osteoarthritis:
711 relation to clinical assessment (ICRS Grade). *Osteoarthritis Cartil*
712 */ OARS, Osteoarthr Res Soc* 13:958–963

713 29. Brittberg M et al., ICRS Cartilage Injury Evaluation Package.
714 Proceedings of 3rd ICRS meeting, Göteborg, Sweden., 2000.
715 Available online: [http://www.cartilage.org/_files/contentmanagement/](http://www.cartilage.org/_files/contentmanagement/ICRS_evaluation.pdf)
716 [ICRS_evaluation.pdf](http://www.cartilage.org/_files/contentmanagement/ICRS_evaluation.pdf)

717 30. Hoetker MS, Goetz M (2013) Molecular imaging in endoscopy. *U*
718 *Eur Gastroenterol J* 1:84–92

719 31. Popp J, Schmitt M (2013) The Many facets of Raman Spectroscopy
720 in Biophotonics. In: *Optics in the Life Sciences*, Waikoloa Beach,
Hawaii. OSA Technical Digest (online). Optical Society of 721
America, p MT1C.1 722

32. Mainil-Varlet P, Aigner T, Brittberg M, Bullough P, Hollander A, 723
Hunziker E, Kandel R, Nehrer S, Pritzker K, Roberts S, Stauffer E 724
(2003) Histological assessment of cartilage repair: a report by the 725
Histology Endpoint Committee of the International Cartilage 726
Repair Society (ICRS). *J Bone Joint Surg Am Vol* 85-A(Suppl 2): 727
45–57 728

33. Severcan F, Haris PI (2012) *Vibrational Spectroscopy in Diagnosis*
729 *and Screening*. *Advances in Biomedical Spectroscopy*, Vol 6. IOS 730
Press 731

34. Salzer R, Siesler HW (2009) *Infrared and Raman Spectroscopic*
732 *Imaging*. eds., Wiley-VCH, Weinheim, Germany 733

35. Meade A, Clarke C, Draux F, Sockalingum G, Manfait M, Lyng F, 734
Byrne H (2010) Studies of chemical fixation effects in human cell 735
lines using Raman microspectroscopy. *Anal Bioanal Chem* 396: 736
1781–1791 737

36. Kunstar A (2012) *Confocal Raman microspectroscopy: application*
738 *in cartilage tissue engineering*. PhD Thesis., University of Twente, 739
Enschede, The Netherlands 740

37. Huang Z, McWilliams A, Lam S, English J, McLean DI, Lui H, 741
Zeng H (2003) Effect of formalin fixation on the near-infrared 742
Raman spectroscopy of normal and cancerous human bronchial 743
tissues. *Int J Oncol* 23:649–655 744

38. Dubessy J, Rull F, Sharma S (2012) *Instrumentation in Raman*
745 *spectroscopy; elementary theory and practice (in Applications of*
746 *Raman spectroscopy to earth sciences and cultural heritage)*. *Eur*
747 *Mineral Union Notes Mineral* 12:83–172 748

39. Esmonde-White FWL, Schulmerich MV, Esmonde-White KA, 749
Morris MD (2009) Automated Raman spectral preprocessing of 750
bone and other musculoskeletal tissues. *Proc. SPIE:* 716605– 751
716610 752

40. Savitzky A, Golay MJE (1964) Smoothing and differentiation of 753
data by simplified least squares procedures. *Anal Chem* 36:1627– 754
1639 755

41. Barman I, Singh GP, Dasari RR, Feld MS (2009) Turbidity- 756
corrected Raman spectroscopy for blood analyte detection. *Anal*
757 *Chem* 81:4233–4240 758

42. Zhao J, Lui H, McLean DI, Zeng H (2007) Automated autofluores- 759
cence background subtraction algorithm for biomedical Raman 760
spectroscopy. *Appl Spectrosc* 61:1225–1232 761

43. Barman I, Kong CR, Singh GP, Dasari RR (2011) Effect of 762
photobleaching on calibration model development in biological 763
Raman spectroscopy. *J Biomed Opt* 16:011004 764

44. Kumar R, Singh GP, Barman I, Dingari NC, Nabi G (2013) A facile 765
and real-time spectroscopic method for biofluid analysis in point- 766
of-care diagnostics. *Bioanalysis* 5:1853–1861 767

45. Bugay DE (2001) Characterization of the solid-state: spectroscopic 768
techniques. *Adv Drug Deliv Rev* 48:43–65 769

46. McCreery RL (2000) *Raman spectroscopy for chemical analysis*. 770
Wiley-Interscience, New York 771

47. Rösch P, Harz M, Schmitt M, Popp J (2005) Raman spectroscopic 772
identification of single yeast cells. *J Raman Spectrosc* 36:377–379 773

48. Myakalwar AK, Sreedhar S, Barman I, Dingari NC, Venugopal Rao 774
S, Prem Kiran P, Tewari SP, Manoj Kumar G (2011) Laser-induced 775
breakdown spectroscopy-based investigation and classification of 776
pharmaceutical tablets using multivariate chemometric analysis. 777
Talanta 87:53–59 778

49. Smith E, Dent G (2005) *Modern Raman spectroscopy: a practical*
779 *approach*. Wiley. 780

50. Stone N, Kendall C, Smith J, Crow P, Barr H (2004) Raman spec- 781
troscopy for identification of epithelial cancers. *Faraday Discuss*
782 126:141–157, **discussion 169–183** 783

51. Stone N, Stavroulaki P, Kendall C, Birchall M, Barr H (2000) 784
Raman spectroscopy for early detection of laryngeal malignancy: 785
preliminary results. *Laryngoscope* 110:1756–1763 786

787 52. Barman I, Dingari NC, Singh GP, Kumar R, Lang S, Nabi G (2012) 822
 788 Selective sampling using confocal Raman spectroscopy provides 823
 789 enhanced specificity for urinary bladder cancer diagnosis. *Anal* 824
 790 *Bioanal Chem* 404:3091–3099 825
 791 53. Rosenberg L (1971) Chemical basis for the histological use of saf- 826
 792 ranin O in the study of articular cartilage. *J Bone Joint Surg Am Vol* 827
 793 53:69–82 828
 794 54. Pritzker KP, Gay S, Jimenez SA, Ostergaard K, Pelletier JP, Revell 829
 795 PA, Salter D, van den Berg WB (2006) Osteoarthritis cartilage 830
 796 histopathology: grading and staging. *Osteoarthritis Cartil / OARS,* 831
 797 *Osteoarthr Res Soc* 14:13–29 832
 798 55. Dehring KA, Smukler AR, Roessler BJ, Morris MD (2006) 833
 799 Correlating changes in collagen secondary structure with aging 834
 800 and defective type II collagen by Raman spectroscopy. *Appl* 835
 801 *Spectrosc* 60:366–372 836
 802 56. Takahashi Y, Sugano N, Takao M, Sakai T, Nishii T, Pezzotti G 837
 803 (2014) Raman spectroscopy investigation of load-assisted micro- 838
 804 structural alterations in human knee cartilage: preliminary study 839
 805 into diagnostic potential for osteoarthritis. *J Mech Behav Biomed* 840
 806 *Mater* 31:77–85 841
 807 57. Bonifacio A, Sergio V (2010) Effects of sample orientation in 842
 808 Raman microspectroscopy of collagen fibers and their impact on 843
 809 the interpretation of the amide III band. *Vib Spectrosc* 53:314–317 844
 810 58. Lednev IK, Karnoup AS, Sparrow MC, Asher SA (1999) 845
 811 Nanosecond UV resonance Raman examination of initial steps in 846
 812 α -helix secondary structure evolution. In: Puppels GJ, Otto C (eds) 847
 813 Greve J. *Spectroscopy of Biological Molecules, New Directions.* 848
 814 Springer Netherlands, pp 11–12 849
 815 59. Abdi H (2007) The eigen-decomposition: eigenvalues and eigen- 850
 816 vectors. Salkind NJ (Ed.), *Encyclopedia of Measurement and* 851
 817 *Statistics.* Sage Publications 852
 818 60. Mobili P, Londero P, De Antoni G, Gomez-Zavaglia A (2010) 853
 819 Multivariate analysis of Raman spectra applied to microbiology: 854
 820 discrimination of microorganisms at the species level. *Revista*
 821 *Mexicana De Fisica* 56:378–385

61. Sahu A, Dalal K, Naglot S, Aggarwal P, Murali Krishna C (2013) 822
 Serum based diagnosis of asthma using Raman spectroscopy: an 823
 early phase pilot study. *PLoS One* 8 824
 62. Knudson CB, Knudson W (2001) Cartilage proteoglycans. *Semin* 825
Cell Dev Biol 12(2):69–78. doi:10.1006/scdb.2000.0243 826
 63. Fischer WB, Eysel HH (1992) Polarized Raman spectra and intens- 827
 ities of aromatic amino acids phenylalanine, tyrosine and trypto- 828
 phan. *Spectrochim Acta A: Mol Spectrosc* 48(5):725–732 829
 64. Rizkalla G, Reiner A, Bogoch E, Poole AR (1992) Studies of the 830
 articular cartilage proteoglycan aggrecan in health and osteoarthri- 831
 tis. Evidence for molecular heterogeneity and extensive molecular 832
 changes in disease. *J Clin Invest* 90(6):2268–2277 833
 65. Thompson RC Jr, Oegema TR Jr (1979) Metabolic activity of art- 834
 icular cartilage in osteoarthritis. An in vitro study. *J Bone Joint* 835
Surg Am Vol 61(3):407–416 836
 66. Mankin HJ, Dorfman H, Lippiello L, Zarins A (1971) Biochemical 837
 and metabolic abnormalities in articular cartilage from osteo- 838
 arthritic human hips. II. Correlation of morphology with biochem- 839
 ical and metabolic data. *J Bone Joint Surg Am Vol* 53(3):523–537 840
 67. Radin EL, Rose RM (1986) Role of subchondral bone in the initi- 841
 ation and progression of cartilage damage. *Clin Orthop Relat Res* 842
 213:34–40 843
 68. Burr DB (2004) Anatomy and physiology of the mineralized tis- 844
 sues: role in the pathogenesis of osteoarthritis. *Osteoarthritis Cartil,* 845
Osteoarthr Res Soc 12(Suppl A):S20–30 846
 69. Buck RJ, Wirth W, Dreher D, Nevitt M, Eckstein F (2013) 847
 Frequency and spatial distribution of cartilage thickness change in 848
 knee osteoarthritis and its relation to clinical and radiographic co- 849
 variates - data from the osteoarthritis initiative. *Osteoarthritis Cartil,* 850
Osteoarthr Res Soc 21(1):102–109 851
 70. Esmonde-White KA, Esmonde-White FW, Morris MD, Roessler 852
 BJ (2011) Fiber-optic Raman spectroscopy of joint tissues. 853
Analyst 136(8):1675–1685 854

UNCORRECTED PROOF